Leptons with $E > 200$ MeV trapped in the Earth's radiation belts

E. Fiandrini, G. Esposito, B. Bertucci, B. Alpat, R. Battiston, W. J. Burger, G. Lamanna, and P. Zuccon

Istituto Nazionale Fisica Nucleare, University of Perugia, Perugia, Italy

Received 14 June 2001; revised 17 September 2001; accepted 18 September 2001; published 1 June 2002.

[1] For the first time, accurate measurements of electron and positron fluxes in the energy range 0.2–10 GeV have been performed with the Alpha Magnetic Spectrometer (AMS) at altitudes of 370–390 km in the geographic latitude interval ±51.7°. We describe the observed under-cutoff lepton fluxes outside the region of the South Atlantic Anomaly. The separation in quasi-trapped, long-lifetime (O(10 s)), and albedo, short-lifetime (O(100 ms)), components is explained in terms of the drift shell populations observed by AMS. A significantly higher relative abundance of positrons with respect to electrons is seen in the quasi-trapped population. The flux maps as a function of the canonical adiabatic variables L, α_0 are presented for the interval $0.95 < L < 3$, $0° < \alpha_0 < 90°$ for electrons ($E < 10$ GeV) and positrons ($E < 3$ GeV). The results are compared to existing data at lower energies. The properties of the observed under-cutoff particles are also investigated in terms of their residence times and geographical origin. *INDEX TERMS:* 2720 Magnetospheric Physics: Energetic particles, trapped; 7807 Space Plasma Physics: Charged particle motion and acceleration; 2104 Interplanetary Physics: Cosmic rays; 2116 Interplanetary Physics: Energetic particles, planetary; *KEYWORDS:* lepton fluxes, radiation belts, AMS, trapped particles

1. Introduction

[2] Evidence for high-energy (up to a few hundred MeV) electrons and positrons trapped below the Inner Van Allen Belts has been published during the last 20 years. The existing experimental data in the energy range of 0.04–200 MeV come from satellites covering a large range of adiabatic variables [*Voronov et al.*, 1987; *Galper et al.*, 1986; *Akimov et al.*, 1987; *Heynderickx et al.*, 1996]. Additional information, at relatively higher energies, is furnished by balloon-borne experiments [*Verma*, 1967; *Barwick et al.*, 1998]; however, these data cover a more limited spatial range and have larger uncertanties due to the shorter exposure times and the presence of background from atmospheric showers.

[3] Although the magnetic trapping mechanism is well understood, a complete description of the phenomena, including the mechanisms responsible for the injection and depletion of the belts as well as those determining the energy spectra, is lacking, particularly for energies above a few hundred MeV. At lower energies, models are available for leptons and protons [*Vette*, 1991; *Getselev et al.*, 1991] based on the data provided by satellite campaigns, which are continuously updated for instance in the context of the Trapped Radiation Environment Development project (TREND; http://www.magnet.oma.be/home/trend/trend.html, http://www.magnet.oma.be/-unilib.html, and http://www.spenvis.oma.be/spenvis).

[4] At higher energies the existing data come from measurements carried out by the Moscow Engineering Physics Institute. These data, taken at altitudes ranging from 300 to 1000 km with different instruments placed on satellites and the Mir station [*Voronov et al.*, 1987; *Galper et al.*, 1986; *Akimov et al.*, 1987], established the existence of O(100 MeV) trapped leptons both in the Inner Van Allen Belts (stably trapped) and in the region below (quasi-trapped), and they determined their charge composition [*Averin et al.*, 1988; *Galper et al.*, 1996]. At these altitudes the shell structure is strongly distorted in the vicinity of the South Atlantic Anomaly (SAA), and consequently the observations are sensitive to different regions of trapped particles: the Inner Van Allen belts over the SAA and quasi-trapping belts outside of the SAA. An example of the shell structure relevant at these altitudes is shown in Figure 1: the shell evolves essentially above the atmosphere which it intercepts around the SAA. The Russian measurements concern mainly the region of the SAA; very little data are available at the corresponding altitudes outside the SAA.

[5] The measured ratio of e^+ to e^- is found to depend strongly on the observed population type. In the SAA, electrons dominate the positrons by a factor ~10, a ratio similar to that observed for the cosmic fluxes, while outside the SAA the two fluxes are similar and comparable to the e^+ flux inside the SAA [*Galper et al.*, 1996]. However, the situation is not completely clear, since other groups report a lower e^- excess (~2) for the SAA [*Kurnosova et al.*, 1991].

[6] In the following we use the high statistics data sample collected by the AMS experiment in 1998, for a detailed study of the under-cutoff lepton fluxes in the O(1 GeV) energy range. The data are analyzed in terms of the canonical invariant coordinates characterizing the particle motion in the magnetic field: the L shell parameter, the equivalent magnetic equatorial radius of the shell, the equatorial pitch angle, α_0, of the momentum **p** with the **B** field, and the mirror field B_m at which the motion reflection occurs during bouncing [*McIlwain*, 1961; *Hilton*, 1971].

2. AMS and the STS 91 Flight

[7] The Alpha Magnetic Spectrometer (AMS), equipped with a double-sided silicon microstrip tracker, has an analyzing power of $BD^2 = 0.14$ Tm^2, where B is the magnetic field intensity and D is the typical path length in the field. A plastic scintillator time-of-flight system measures the particle velocity and an Aerogel Threshold Cerenkov counter provides the discrimination between proton and $e^{\pm}$. In the present analysis a fiducial cone with a 28° half-angle opening aperture was defined to select the

0148-0227/02/2001JA900151

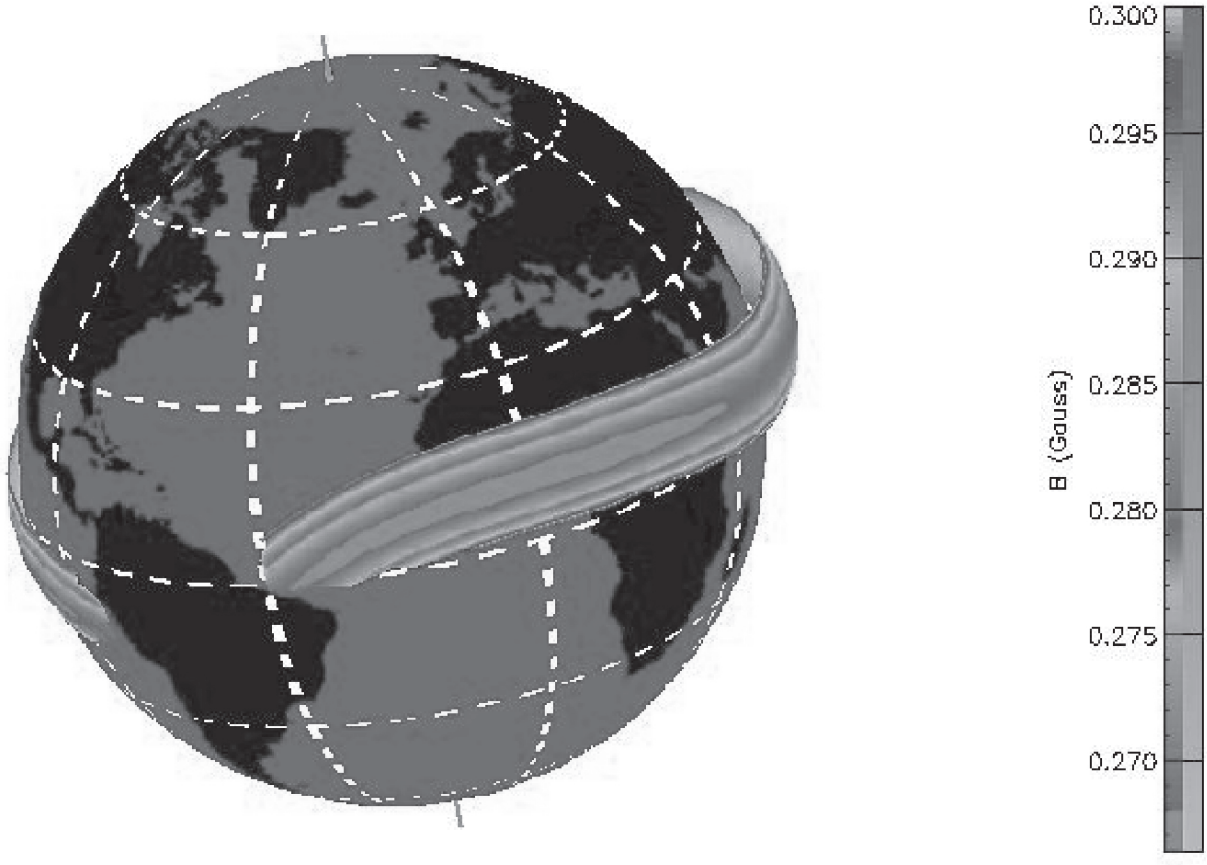

Figure 1. Example of the geometrical surface of a drift shell in a quasi-trapping belt. Notice the typical nonclosed structure, in the vicinity of the South Atlantic Anomaly (SAA) (Space Environment Information System (SPENVIS) package, TREND program). See color verion of this figure at back of this issue.

leptons entering the detector, resulting in an average acceptance of $\sim$160 cm^2 sr. Further details on the detector performance, lepton selection, and background estimation can be found in the work of *Alcaraz et al.* [2000, and references therein].

[8] The AMS was operated on the shuttle Discovery during a 10-day flight, beginning on 2 June 1998 (NASA mission STS 91). The detector, which was not magnetically stabilized, recorded data during 17, 6, 7, and 14 hours, pointing at 0°, 20°, 45°, and 180°, respectively, from the local zenith direction. The results presented here are obtained from the data of these periods. The orbital inclination was 51.7° in geographic coordinates, at a geodesic altitude of 370–390 km. Trigger rates varied between 100 and 700 Hz. The data from the SAA are excluded in our analysis.

[9] The shuttle position and the AMS orientation in geographic coordinates were provided continuously during the flight by the telemetry data. The values of L, α_0, and B_m of the detected leptons were calculated using the UNILIB package (TREND project) with a realistic magnetic field model, including both the internal and the external contributions (International Geomagnetic Reference Field (IGRF), http://nssdc.gsfc.nasa.gov/space/model/magnetos/igrf.html) [*Tsyganenko*, 1982]. The AMS field of view (FOV) in the (L, α_0) coordinate space is determined both by the orbit parameters (geographic locations and flying attitude) and by the finite acceptance of the detector.

[10] A simulation was developed to determine the AMS FOV along the orbit and evaluate the effects due to the finite detector acceptance. The results are shown in Figure 2. The (α_0, L) coverage is similar for the different attitudes. The finite acceptance of the detector influences essentially the definition of the lower contour.

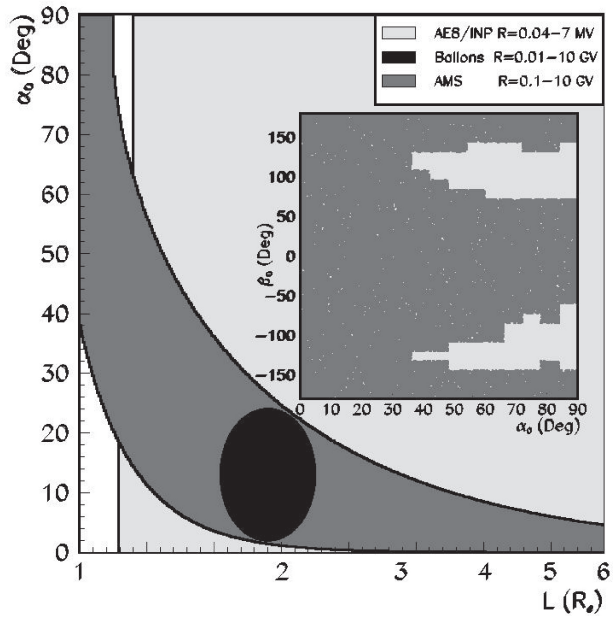

Figure 2. Comparison of the field of view of the Alpha Magnetic Spectrometer (AMS) with balloons and satellite measurements in (L, α_0). In the insert plot the AMS coverage in β_0 versus α_0 is shown. AEB, Aerospace Electrons model 8; INP, Institute of Nuclear Physics.

The upper limit is imposed by the orbital altitude and is described by the relation $\alpha_0 = \sqrt{0.311/L^3 B_m}$, where B_m = 0.225 G is the minimum mirror field encountered along the AMS orbit. Since the particles which are mirroring above the AMS altitude cannot be observed, particles with large equatorial pitch angles can only be detected at low L values ($L \leq 1.2$). At larger L, only particles with a smaller α_0 can be observed. Because of the fixed flight attitudes, the azimuthal β_0 coverage in the local magnetic reference frame ($\hat{z} = \hat{B}$, $\hat{x} = (\widehat{\nabla B})_\perp$, $\hat{y} = \hat{z} \times \hat{x}$) was not complete, as shown in the insert plot of Figure 2.

3. Data Analysis

[11] To reject the cosmic component of the measured lepton fluxes, the lepton trajectories in the Earth's magnetic field were traced using a fourth-order Runge Kutta method with adaptive step size. The equation of the motion was solved numerically, and a particle was classified as trapped if its trajectory reached an altitude of 40 km [*Alcaraz et al.*, 2000], taken as the dense atmosphere limit where the total probability of interaction is 50%, before its detection in AMS. Although satisfactory in most cases, this approach is less stable when the particle rigidity falls in the penumbra region, close to the cutoff value. In this case the trajectories become chaotic, and small uncertainties in the reconstructed rigidity and in the B field can lead to a misclassification. The validity of the adiabatic approach requires the parameter $\varepsilon = \rho/R$ to be small [*Il'in et al.*, 1986; *Schulz*, 1996], where ρ is the equatorial Larmor radius of a particle and R is the field radius of curvature at the equator. *Il'in et al.* [1986] show that the motion becomes chaotic if $\varepsilon \geq 0.1$. The AMS data are consistent with this limit even though the detected particle energies are relatively high. To avoid such effects, we have defined an effective cutoff, $R_{\rm eff}$, as the maximum rigidity value at a given magnetic latitude θ_m for which no traced lepton was found to be of cosmic origin. The $R_{\rm eff}$ values as a function of the magnetic latitude are shown as solid triangles in Figure 3. We rejected from our sample all particles with $R > R_{\rm eff}$.

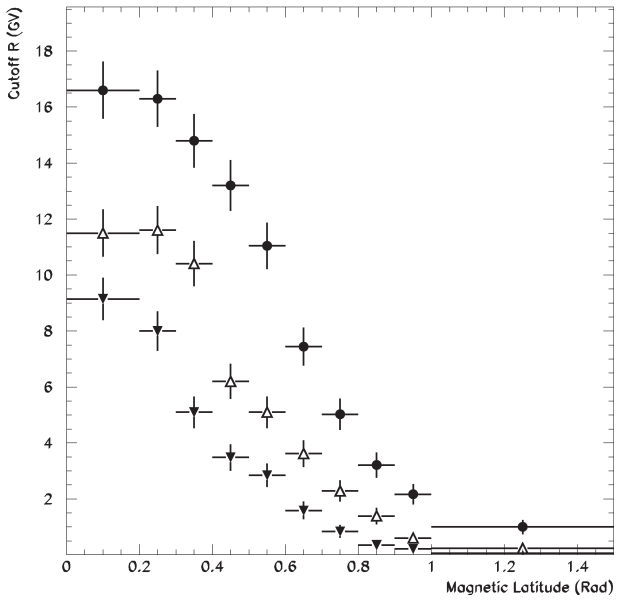

Figure 3. Effective cutoff as a function of the magnetic latitude (solid triangles), defined as the lowest rigidity below which no primaries are found. The highest rigidities above which all the leptons are primaries (points) and 50% are secondaries (open triangles) are also shown.

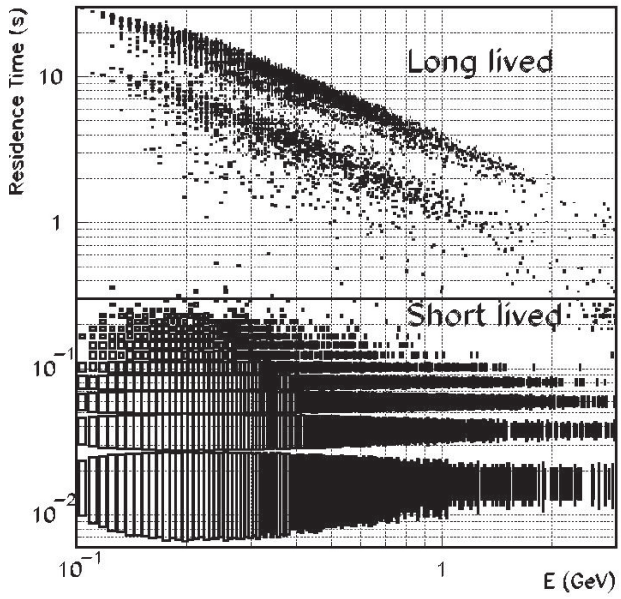

Figure 4. Residence time versus energy for e^+. The same structure is observed for e^-.

[12] The residence time, T_f, of the under-cutoff particles is computed, i.e., the total time spent by each particle in its motion above the atmosphere, before and after detection. The geographical location where the trajectories intercept the atmosphere determines the leptons production and impact points, defined as the position from which the particle leaves or enters the atmosphere.

[13] The residence time distribution as a function of energy is shown for positrons in Figure 4; the same behavior is observed for

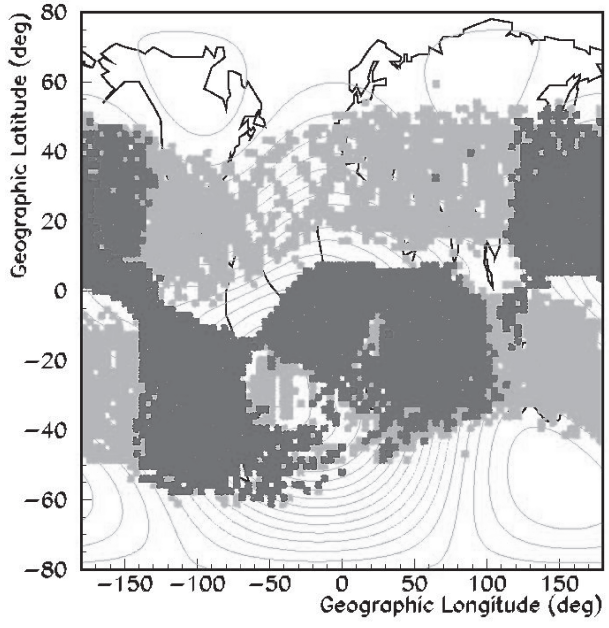

Figure 5. Geographical positions of production and impact points in the atmosphere. Yellow bands show the distribution for short-lived e^-, and red/blue bands show the production/impact distribution for long-lived e^-. A similar but complementary structure is observed for e^+. See color verion of this figure at back of this issue.

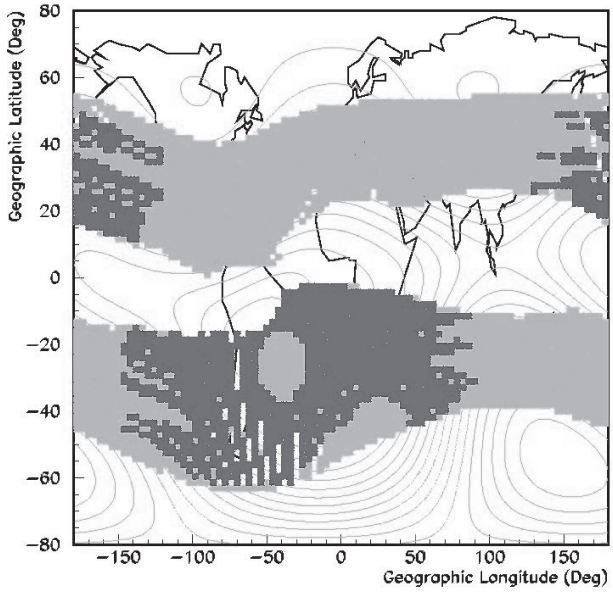

Figure 6. Distribution of intersection points with atmosphere for the drift shells crossed by AMS. The yellow region corresponds to shells with $B_m \geq 0.48L^{0.41}$ G, and the blue region corresponds to shells with $B_m \leq 0.48L^{0.41}$ G. See color verion of this figure at back of this issue.

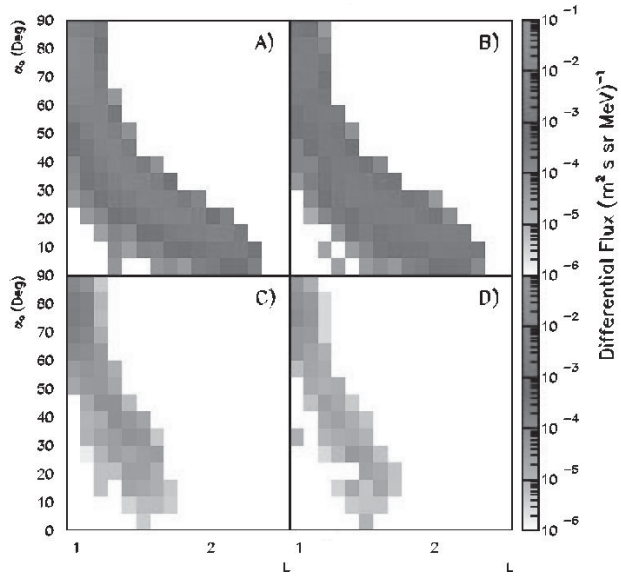

Figure 7. Flux maps for two different energy bins: (a, b) e^+ and e^- between $0.315 \leq E \leq 0.486$ GeV and (c, d) e^+ and e^- between $1.77 \leq E \leq 2.73$ GeV. See color verion of this figure at back of this issue.

electrons. All observed leptons have residence times below ~30 s, with 52% of the e^- and 38% of the e^+ having a $T_f < 0.3$ s independent of their energy. The corresponding impact/production points are spread, for both e^+ and e^-, over two bands on either side of the magnetic equator, as indicated by the the yellow bands in Figure 5. A scaling law, $T_f \approx E^{-1}$, is observed for the remaining leptons: they are disposed in two diagonal bands separated by a difference in T_f of $\approx 2.2/E$ s. The impact/production points for e^+ are localized in the red/blue spots of Figure 5: the same regions describe, respectively, the production/impact regions of e^-.

[14] The data have been previously published by the AMS collaboration [*Alcaraz et al.*, 2000] using the terminology of short-lived and long-lived to classify the particles with T_f below and above 0.2 s. However, no interpretation was advanced at that time to describe the observed distributions. *Lipari* [2001] has discussed the AMS results qualitatively.

[15] An exhaustive explanation must take into account the geometry of the shells relevant to the AMS measurements and the fact that these shells evolve partially under the atmosphere; therefore no permanent trapping can occur. The residence times are determined by the periodicities of the drift (τ_d) and bouncing ($\tau_b \ll \tau_d$) motions; the type of motion which dominates depends on the relative fraction of the shell mirror points lying above the atmosphere.

[16] The impact/production points correspond to the intersection of the shell surfaces with the atmosphere, as shown in Figure 6, where particles generated in interactions are injected into the shells. Long-lived and short-lived particles move along shells with different values of B_m, or equivalently α_0, which determine the mirror height on each field line. For high B_m values, or low α_0, the mirror height is very low, and the shells penetrate into the atmosphere at nearly all longitudes. Therefore particles are absorbed shortly after injection in the shells. This is shown by the yellow bands in Figure 6 corresponding to shells with $B_m \geq 0.48$, $L^{0.41}$ G; they reproduce well the impact/production points for short-lived leptons. When B_m is lower, or α_0 is closer to 90°, the shells descend below the atmosphere only in the vicinity of the SAA, indicated by the blue regions in Figure 6, which correspond to shells with $B_m \leq 0.48$, $L^{0.41}$ G, and reproduce the impact/production points of the long-lived leptons. These particles can drift nearly an entire revolution before absorption in the atmosphere. For the short-lived component the bouncing motion is dominant; the residence time is given by $T_f = k\tau_b$, where τ_b is the bouncing motion period and k is an integer or half-integer

Table 1. Bin Limits Used for AMS Data

	Number of Bins	Limit	Bin Width
E	9	0.2–10 GeV	0.187 (log)
L	16	0.95–3.	0.031 (log)
α_0	15	0°–90°.	6° (lin)

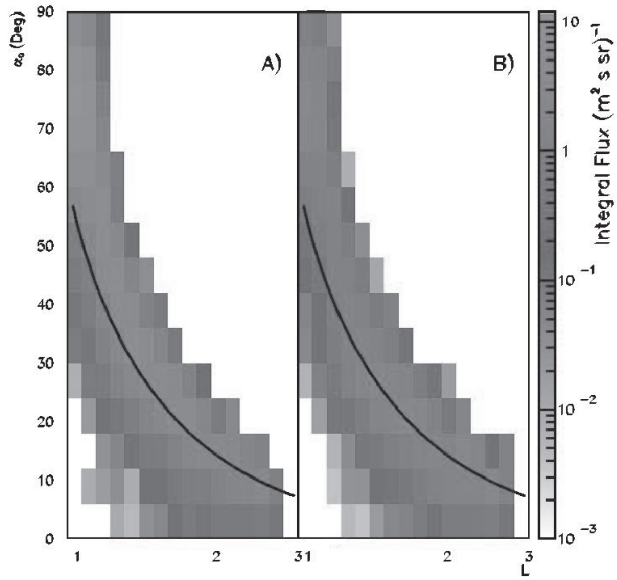

Figure 8. The integrated flux maps for (a) e^+ and (b) e^- between $0.205 \leq E \leq 2.73$ GeV. The line shows the curve below which no quasi-trapped leptons are found. See color verion of this figure at back of this issue.

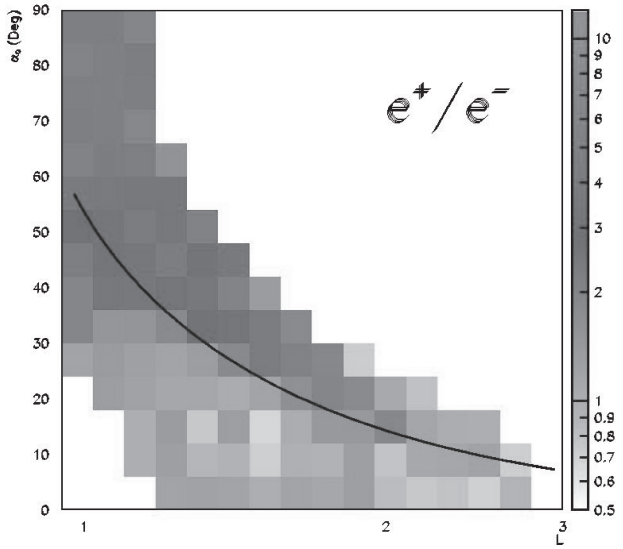

Figure 9. The integrated e^+/e^- ratio between $0.205 \leq E \leq 2.73$ GeV. The line shows the curve below which no quasi-trapped leptons are found. See color verion of this figure at back of this issue.

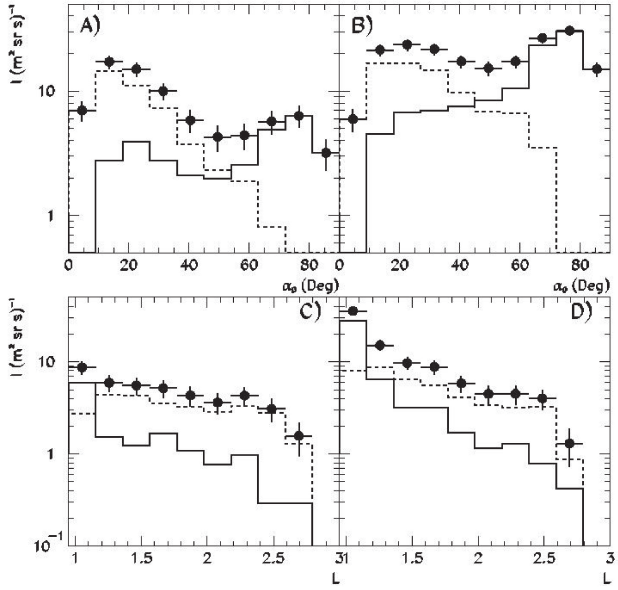

Figure 10. The integrated flux as a function of α_0 and as a function of L for (a, c) e^- and (b, d) e^+ between $0.205 \leq E \leq 2.73$ GeV. The solid line shows the long-lived component, the dashed line shows the short-lived component, and the points show the total flux.

between $1/2 \leq k \leq 5$. In the dipolar field model, τ_b is given by $\tau_b = f(\alpha_0)L$, where f is a slowly varying function of α_0; the upper limit is $\tau \sim 300$ ms for the AMS data. The substructure seen in the short-lived component of Figure 4 is due to the discrete values of k and the different L shells crossed during the AMS orbits. For the long-lived component the drift motion is dominant, and $T_f = k' \tau_d$, where τ_d is the drift motion period, $\tau_d = f'(\alpha_0)/EL$, where f' is a slowly varying function of α_0, and k′ is a number less than 1, corresponding to the fraction of a complete drift shell spanned by a particle. The two bands seen for the long-lived component of Figure 4 correspond to fractions of ~0.65 and ~0.25 of a complete drift.

4. AMS Results

[17] For the description of under-cutoff fluxes the energy E, the L parameter, and the equatorial pitch angle α_0 were used (this is preferred to B_m since limited to 0°–90°). A three-dimensional grid (E, L, α_0) was defined to build flux maps. A linear binning in α_0 and logarithmic variable size for L and E bins were chosen to optimize the statistics in each bin. The interval limits and bin widths are listed in Table 1.

[18] The flux maps in (L, α_0) at constant E give the distribution of particle populations at the altitude of AMS. Nine maps at constant E have been made. Two different maps for two different energy bins of e^+ and e^- are shown in Figure 7. The flux is limited by the cutoff rigidity R_c: on a given shell, only particles with $R \leq R_c$ are allowed to populate the shell; hence lower and lower energy particles populate higher and higher shells.

[19] The e^+, e^- flux maps and their ratio in the energy interval 0.2–2.7 GeV are shown in Figures 8 and 9, respectively. The solid line in the two plots identifies the lower boundary in (L, α_0) below which no leptons can be found with residence times larger than 0.3 s and is defined by the relation $\sin \alpha_c = 0.8L^{-1.7}$. Above the curve, for increasing values of α_0, the long-lived component of the fluxes becomes increasingly dominant. This is demonstrated in Figure 10, where the same distributions, integrated over α_0 (Figures 10c and 10d) and L (Figures 10a and 10b), are shown. The contributions of leptons with $T_f < 0.3$ s and $T_f > 0.3$ s are represented with dashed and solid lines, respectively. Above $\alpha_0 > 60°$ the flux is due substantially to the long-lived component; the e^+ flux represents ≈80% of the total leptonic flux, while at the same level or less than the e^- flux in the low α_0 region. The long-lived component dominates only at very low L values, where the positron excess is more pronounced.

[20] This is seen clearly in the energy spectra for particles with $\alpha_0 \geq 70°$, shown in Figure 11, which is superimposed with the lower energy measurements from MARYA [*Galper et al.*, 1996]. At large pitch angles the e^+ flux is higher than e^- flux by a factor ~4.5, in contrast to MARYA data which indicate the same level of flux for both lepton charges.

[21] The critical pitch angle α_c can explain the presence of the two well-separated components in the residence time: the albedo

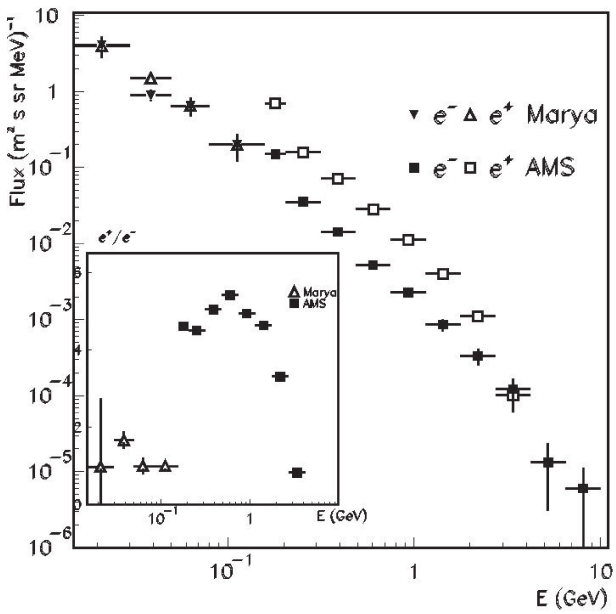

Figure 11. Energy spectrum comparison between AMS and Marya for e^+ and e^- for particles with $\alpha_0 \geq 70°$. In the insert plot, the e^+/e^- ratio comparison is shown.

(short-lived) and quasi-trapped (long-lived) ones. Particles inside a cone with a half-opening angle α_c around **B** will enter the atmosphere every bounce and therefore will disappear rapidly, while those outside it will enter the atmosphere only near SAA. In this context, α_c can be defined as the "equatorial bouncing loss cone angle," i.e., the largest pitch angle for which particles enter the atmosphere every bounce. Taking into account α_c, the residence time can be written as $T_f = k\tau_b\theta(-\alpha_0 + \alpha_c) + k'\tau_d\theta(\alpha_0 - \alpha_c)$, where θ is the Heavyside step function. The two terms correspond to very different components of motion ($\tau_b \ll \tau_d$), according to the bounce loss cone on that field line. Furthermore, all the observed particles are in a drift loss cone angle since all of them enter the atmosphere within one revolution after injection. This explains the absence of a peak at 90° in the pitch angle distributions of Figures 10a and 10b.

5. Discussion

[22] The AMS data establish the existence of leptonic radiation belts, with particle energies in the range of several GeV, below the Inner Van Allen belts. The particles populating these belts are not stably trapped since the corresponding drift shells are not closed over above the atmosphere in the region of the SAA.

[23] At any given L a critical value of the equatorial pitch angle, α_c, the bouncing loss cone, can be defined to distinguish the long-lived, or quasi-trapped, and the short-lived, or albedo, components of the fluxes. The same value is found to separate the regions where the e^+/e^- ratio is above or around unity: the charge composition shows a clear dominance of positively charged leptons in a definite region of the (L,α_0) space above $\alpha_c(L)$.

[24] The observed behavior distinguishes these belts from the Inner Van Allen belts and limits the possible injection/loss mechanisms to those acting on a timescale much shorter than the typical particle residence times. Mechanisms related to Coulomb scattering, like pitch angle diffusion, are ruled out since they imply much longer timescales. Moreover, the observed charge ratio distribution provides an important constraint for potential models.

[25] The interaction of primary cosmic rays and inner radiation belt protons with atmospheric nuclei in the regions of shell intersection with the atmosphere is a natural mechanism for the production of secondary leptons through the π-μ-e or π-γ-e decay chains. This leads to a e^+ excess over e^- and seems suitable to explain the observed charge ratio for the quasi-trapped flux [*Voronov et al.*, 1995a; *Gusev and Pugacheva*, 1982]. However, for the albedo flux the charge ratio is of the order of unity, as seen in Figure 9, and other mechanisms might be present.

[26] Recent Monte Carlo studies based on this mechanism have been able to fully reproduce the under-cutoff proton spectrum reported by AMS [*Derome et al.*, 2000], while a less good agreement for the under-cutoff lepton spectrum [*Derome et al.*, 2001] was obtained. In the work of *Lipari* [2001] the influence of geomagnetic effects, mainly related to the east-west asymmetry for cosmic protons, is taken into account to qualitatively explain the observed charge ratio. However, more refined studies are needed to definitely exclude contributions from other mechanisms, i.e., acceleration processes acting on the leptons resulting from the decays of β-active secondary nuclei and neutrons of albedo and solar origin [*Voronov et al.*, 1995b].

[27] In conclusion, the AMS under-cutoff lepton spectrum can be described naturally in terms of the canonical adiabatic variables associated with the Earth's magnetic field, taking into account the role played by the atmosphere. There are clear indications that π decays can account for the quasi-trapped component of the flux, while the situation is less clear for the albedo component where other processes may contribute.

[28] **Acknowledgments.** We gratefully acknowledge our colleagues in AMS, in particular Z. Ren and V. Choutko. We are also grateful to P. Lipari for useful discussions on the interpretation of the AMS data. We greatly benefited from the software libraries (UNILIB, SPENVIS) developed in the context of the Trapped Radiation Environment Development (TREND) project for ESTEC, and we thank D. Heynderickx for his help. This work has been partially supported by Italian Space Agency (ASI) under the contract ARS 98/47.

[29] Michel Blanc thanks Stefano Orsini and another referee for their assistance in evaluating this paper.

References

Akimov, V. V., et al., The main parameters of gamma ray telescope GAMMA-I, *Conf. Pap. Int. Cosmic Ray Conf. 20th*, *2*, 320–323, 1987.

Alcaraz, J., et al., The AMS collaboration: Leptons in near orbit, *Phys. Lett. B*, *484*, 10–22, 2000.

Averin, S. A., et al.,High-energy electrons in the Earth's radiation belt, *Kosm. Issled.*, *26*(2), 322–324, 1988.

Barwick, S. W., et al., Cosmic ray reentrant electron albedo: High-Energy Antimatter Telescope balloon measurements from Fort Sumner, New Mexico, *J. Geophys. Res.*, *103*, 4817–4823, 1998.

Derome, L., et al., Origin of the high energy proton component below the geomagnetic cutoff in near orbit, *Phys. Lett. B*, *489*, 1–8, 2000.

Derome, L., et al., Origin of leptons in near orbit, *ASTRO-PH/0103474*, Elsevier Sci., New York, 2001.

Galper, A. M., et al., Discovery of high energy electrons in the radiation belt by devices with gas cherenkov counters, *NIM A248*, p. 238, Elsevier Sci., New York, 1986.

Galper, A. M., et al., Electrons with energy exceeding 10 Mev in the Earth's radiation belt, in *Radiation Belts: Models and Standards*, *Geophys. Monogr. Ser.*, vol. 97, edited by J. F. Lemaire, D. Heynderickx, and D. N. Baker, pp. 129–133, AGU, Washington, D.C., 1996.

Getselev, I. V., et al., Model of spatial-energetic distribution of charged particles (protons and electrons) fluxes in the Earth's radiation belts (in Russian), *Preprint MGU-91-37/241*, Inst. of Nucl. Phys., Moscow State Univ., Moscow, 1991.

Gusev, A. A., and G. I. Pugacheva, Formation of albedo electron fluxes in the geomagnetic field, *Geomagn. Aeron.*, *22*, 754–758, 1982.

Heynderickx, D., M. Kruglanski, J. F. Lemaire, and E. J. Daly, A new tool for calculating drift shell averaged atmospheric density, in *Radiation Belts: Models and Standards*, *Geophys. Monogr. Ser.*, vol. 97, edited by J. F. Lemaire, D. Heynderickx, and D. N. Baker, pp. 173–178, AGU, Washington, D.C., 1996.

Hilton, H. H., *L* parameter: A new approximation, *J. Geophys. Res.*, *76*, 6952–6954, 1971.

Il'in, V. D., et al., Stochastic instability of charged particles in a magnetic trap, *Cosmic Res., Engl. Transl.*, *24*, 69–76, 1986.

Kurnosova, L. V., et al., Flux of electrons above 100 MeV in the Earth's radiation belts, *Kosm. Issled.*, *79*(5), 711–716, 1991.

Lipari, P., The fluxes of sub-cutoff particles detected by AMS, the cosmic ray albedo and atmospheric neutrinos, *astro-ph/0101559*, U.S. Natl. Sci. Found., Washington, D.C., 2001.

McIlwain, C. E., Coordinate for mapping the distribution of magnetically trapped particles, *J. Geophys. Res.*, *66*, 3681–3691, 1961.

Schulz, M., Canonical coordinates for radiation-belt modeling, in *Radiation Belts: Models and Standards*, *Geophys. Monogr. Ser.*, vol. 97, edited by J. F. Lemaire, D. Heynderickx, and D. N. Baker, pp. 153–160, AGU, Washington, D.C., 1996.

Tsyganenko, N. A., Determination of magnetospheric model, *Planet. Space Sci.*, *30*, 985–998, 1982.

Tsytovich, V. N., About the acceleration of electrons in the Earth's radiation belts, *Geomagn. Aeron.*, *3*, 616–625, 1963.

Verma, S. D., Measurement of charged splash and re-entrant albedo of the cosmic radiation, *J. Geophys. Res.*, *72*, 915–925, 1967.

Vette, J. I., The AE8 trapped electron model environment, *NSSDC/WDC-A-R&S 91-24*, NASA Goddard Space Flight Cent., Greenbelt, Md., 1991.

Voronov, S. A., et al., High-energy *E*: Electrons and positrons in the Earth's radiation belt, *Geomagn. Aeron.*, *27*,424–426, 1987.

Voronov, S. A., et al., Spectra of albedo electrons and positrons with energy greater than 20 MeV, *Cosmic Res., Engl. Transl.*, *33*, 329–331, 1995a.

Voronov, S. A., et al., Nature of high-energy electrons in Earth's radiation belts, *Cosmic Res., Engl., Transl.*, *33*, 497–499, 1995b.

B. Alpat, R. Battiston, B. Bertucci, W. J. Burger, G. Esposito, E. Fiandrini, G. Lamanna, and P. Zuccon, Department of Physics, Perugia University, and I.N.F.N., Via Pascoli 06100 Perugia, Italy. (Emanuele.Fiandrini@pg.infn.it)

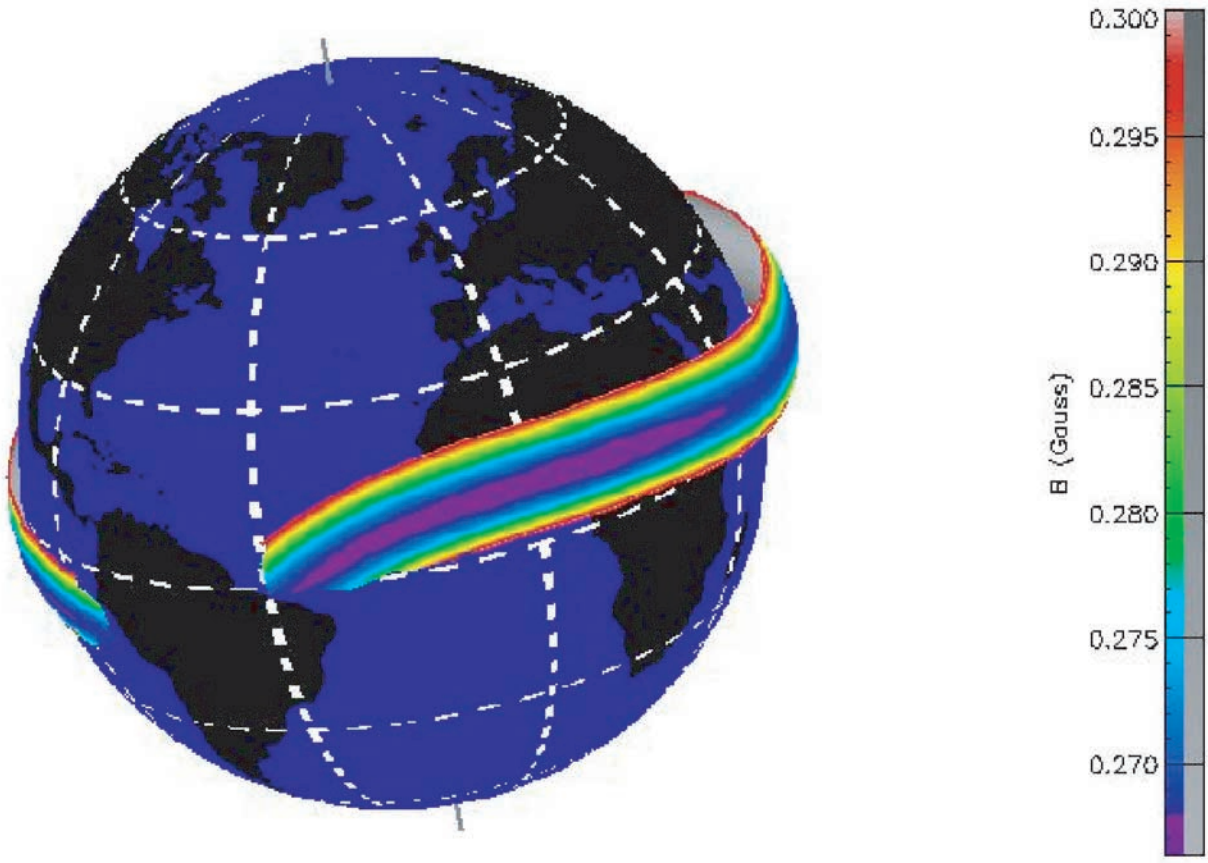

Figure 1. Example of the geometrical surface of a drift shell in a quasi-trapping belt. Notice the typical nonclosed structure, in the vicinity of the South Atlantic Anomaly (SAA) (Space Environment Information System (SPENVIS) package, TREND program).

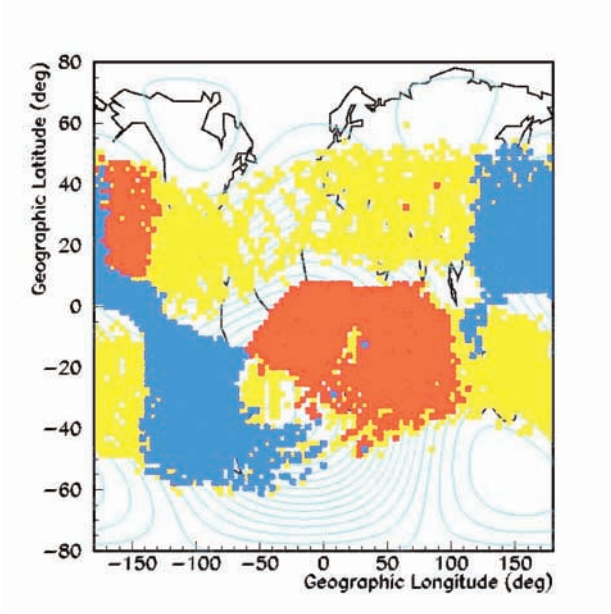

Figure 5. Geographical positions of production and impact points in the atmosphere. Yellow bands show the distribution for short-lived e^-, and red/blue bands show the production/impact distribution for long-lived e^-. A similar but complementary structure is observed for e^+.

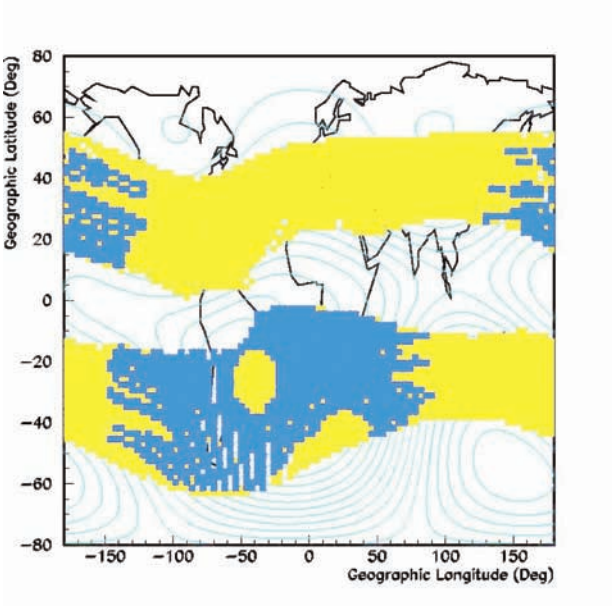

Figure 6. Distribution of intersection points with atmosphere for the drift shells crossed by AMS. The yellow region corresponds to shells with $B_m \geq 0.48\mathrm{L}^{0.41}$ G, and the blue region corresponds to shells with $B_m \leq 0.48\mathrm{L}^{0.41}$ G.

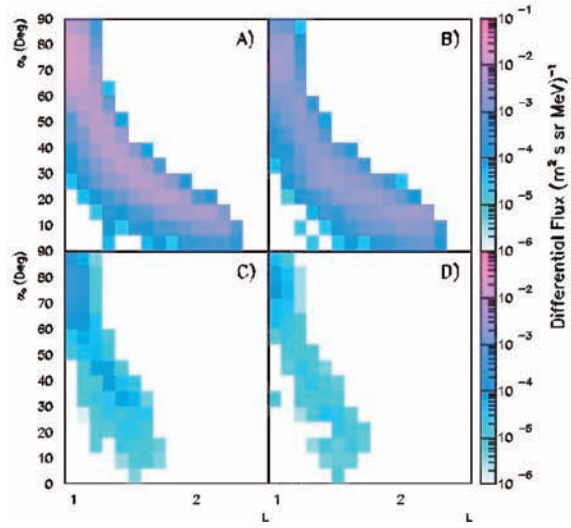

Figure 7. Flux maps for two different energy bins: (a, b) e^+ and e^- between $0.315 \leq E \leq 0.486$ GeV and (c, d) e^+ and e^- between $1.77 \leq E \leq 2.73$ GeV.

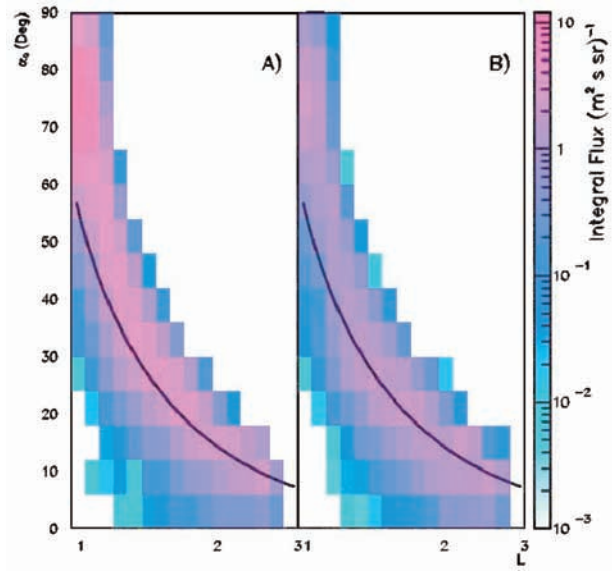

Figure 8. The integrated flux maps for (a) e^+ and (b) e^- between $0.205 \leq E \leq 2.73$ GeV. The line shows the curve below which no quasi-trapped leptons are found.

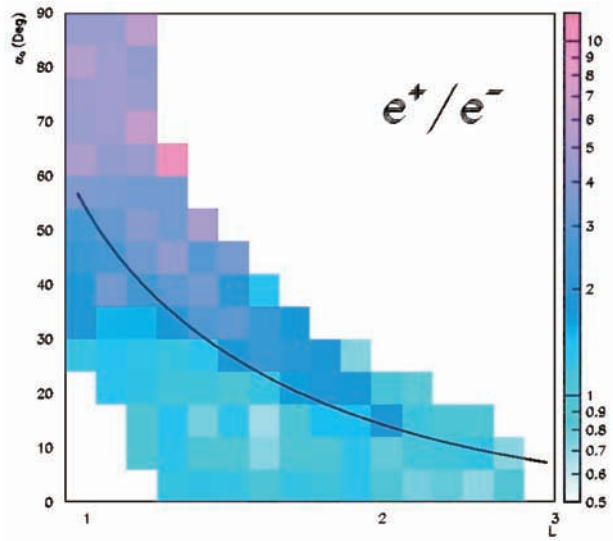

Figure 9. The integrated e^+/e^- ratio between $0.205 \leq E \leq 2.73$ GeV. The line shows the curve below which no quasi-trapped leptons are found.